Regional Studies in Marine Science 39 (2020) 101427

Contents lists available at ScienceDirect

Regional Studies in Marine Science

journal homepage: www.elsevier.com/locate/rsma

Implications of turbulence shear by non-cohesive sediments on the break-up of kaolin flocs

Priya K.L. [a,*], Adarsh S. [a], Venu Chandra [b], S. Haddout [c], Indu M.S. [a]

[a] Department of Civil Engineering, TKM College of Engineering, Kollam, India
[b] Department of Civil Engineering, IIT Madras, India
[c] Department of Physics, Faculty of Science, Ibn Tofail University, Kenitra, Morocco

ARTICLE INFO

Article history:
Received 30 July 2019
Received in revised form 12 August 2020
Accepted 21 August 2020
Available online 24 August 2020

Keywords:
Floc break-up
Turbulence shear
Kaolin
Non-cohesive sediments
Breakage coefficient

ABSTRACT

The present study investigated the role of non-cohesive fraction of sediments on the flocculation of kaolin suspension. The floc characterization was achieved through micro-scale investigations using an image capturing system followed by an image processing technique. Initially, the variations in the characteristics of flocs of kaolin with salinity and turbulence were examined, followed by characterization of flocs under the addition of sand fraction at different proportions (10%, 20%, 40% and 50%). The presence of sand imparts additional shear causing the break-up of macro-flocs of size >100 μm. The variation of floc volume fraction of macro-flocs with turbulence follows a power law, which was used to quantify the additional turbulence shear created by different % of sand. The breakage coefficient of macro-flocs was determined from the experimental results and a relationship for it in terms of turbulence shear is proposed. The developed relationship was further applied to predict the breakage coefficient of macro-flocs due to the addition of sand. The sensitivity analysis conducted between predicted and observed breakage coefficient of macro-flocs due to the addition of sand yielded a correlation coefficient of 0.99. The study proves that the binary breakage model, which propose the break-up of a floc into two equal sized flocs, can be applied to predict breakage coefficient only at intermediate turbulence shear in the range of 20–40 s^{-1}; further it fails to predict the breakage coefficient of macro-flocs in mixed sediment suspensions. The study highlights the role of sand in floc break-up and suggests that the developed model can very well predict the breakage coefficient of macro-flocs in estuaries with mixed sediments as well as at all ranges of turbulence shear encountered in estuaries.

1. Introduction

Cohesive sediments are subjected to complex changes, both physical and chemical, in an estuarine environment due to their electro-chemical and bio-chemical characteristics. These sediments possess surface charge, which undergo changes under the influence of hydrodynamic, chemical and biological factors. As a result, the sediments undergo aggregation and break-up, leading to flocculation. The knowledge of flocculation is pre-requisite for the development of a flocculation model, which can be coupled with sediment transport model for predicting the sediment transport in estuaries and marine environment. The prediction of sediment transport is essential for the management of dredging activities in ports and harbours and other navigation channels. The physical mechanisms influencing flocculation include Brownian motion, turbulent shear and differential settling (Dyer and Manning, 1999; Winterwerp, 2002). Brownian motion plays a significant role only if particle size is less than 1 μm (Winterwerp, 2002) and the suspended sediment concentration (SSC) is much higher than 10 g/L (Burt, 1986) and therefore can be neglected in natural environment (Maggi, 2005). The chances of collision due to differential settling are very small if the particles are more or less of uniform size and are often neglected (Van Leussen, 1994; Winterwerp and Van Kesteren, 2004). The influence of differential settling on flocculation of cohesive sediments in quiescent environments has been highlighted by Gratiot et al. (2017).

The dominant chemical factors that affect flocculation of cohesive sediments are concentration of suspended sediments, composition of suspended sediments, salinity, pH, temperature and viscosity. An increase in flocculation rate and settling velocity of suspended sediments has been reported in many literatures and they proposed a power law for settling velocity with SSC (Van Leussen and Cornelisse, 1992; Priya et al., 2015). The increase in the rate of flocculation with salinity has been well documented (Li et al., 1993; Van Leussen, 1999; Portela et al.,

* Correspondence to: Department of Civil Engineering, TKM College of Engineering, Kollam Kerala, India.
E-mail address: klpriyaram@gmail.com (Priya K.L.).

https://doi.org/10.1016/j.rsma.2020.101427
2352-4855/

2013). When salinity increases, concentration gradient between the Stern layer and Guoy layer of a charged sediment decreases and the thickness of diffuse double layer decreases. Then, the repulsive force between two charged particles occurs only close to the particle, which is overcome by Van der Waals attraction leading to coagulation. An average salinity of 2 ppt for increasing mineral cohesion and aggregation was suggested (Van Leussen, 1988), while Van Leussen (1994) and McAnally (1999) proposed different salt concentration for different minerals. The pH of fluid is also found to influence aggregation by enhancing the ionization of silicon compounds of clay minerals and thereby altering the thickness of double layer. With an increase in pH, the thickness of double layer increases, causing a reduction in cohesion and aggregation. In acidic waters, the double layer compresses resulting in a decrease in zeta potential, getting fully eliminated at a pH∼2 (Vane and Zang, 1997). Temperature and viscosity are symbiotic parameters which affect flocculation. An increase in temperature is said to reduce fluid viscosity, resulting in enhanced molecular motion and inter-particle collision. However, the effect of these are insignificant compared to other parameters and are generally neglected in natural environment. The influence of suspended sediment resuspension and transport on heavy metal distribution has been reported (Priya et al., 2014, 2016).

In the recent years, the role of non-cohesive sediments on the flocculation of cohesive sediments has been studied by researchers (Manning et al., 2010; Cuthbertson et al., 2010; Manning et al., 2011; Cuthbertson et al., 2018). According to the studies conducted by Manning et al. (2010, 2011), non-cohesive sand have a tendency to interact more with smaller denser microflocs than with larger fragile macro-flocs. On the contrary, Cuthbertson et al. (2010) identified that non-cohesive fraction inhibits the aggregation rates and floc sizes of kaolin suspension. Further studies by Cuthbertson et al. (2018) reported that sand fraction reduces initial aggregation rate and floc size at low shear rates, while the effect diminishes at high shear rates. However, these phenomenon were explained on a qualitative basis, even though they attempted modelling the flocculation using population balance model. Thus, the need for quantifying the shear caused by non-cohesive fraction is recognized.

In modelling flocculation of mixed sediment suspensions, the general practice is to adopt a volume double discretization method, wherein a floc of size i breaks into two equal sized flocs, thereby following a binary breakage model. In reality, the floc of size i can break into "n" number of smaller flocs of different sizes. The assumption of binary breakage of flocs will influence the quantification of breakage coefficient (Γ), which is defined as the volume fraction of fragments of size i obtained from j sized flocs (Kusters, 1991; Jackson, 1995; Spicer and Pratsinis, 1996; Ding et al., 2006). Thus, two equal-sized flocs are assumed to form from the break-up of larger floc, thereby leading to a value of 1/2 for the breakage coefficient (Cuthbertson et al., 2018). The present study examines the reliability of the assumption of binary breakage model of flocs of kaolin suspensions due to the shear imparted by non-cohesive sand through experimental observations. A relationship for breakage coefficient in terms of % sand is proposed, which find applications while modelling flocculation of sand–clay suspensions using population balance model. Thus, the main focus of the study is to quantify the turbulence created by the sand fraction and to develop a relationship for breakage coefficient.

2. Materials and methods

2.1. Instrumentation

The instrumentation facilities used for the study include a flocculator, image capturing system and an image processing unit which are described under subsequent sections.

2.1.1. Flocculator

The facility adopted for the study include a flocculator equipped with a variable speed agitator having a single rectangular paddle of 5 cm diameter, placed 20 mm above the bottom of 1 L glass beaker, in which the suspension is placed. The paddle is operated at a turbulence ranging from 0–300 rpm. The turbulence shear (root mean square velocity gradient) G (s^{-1}) was obtained from the power dissipation of the propeller, P (Nagata, 1975; Bouyer et al., 2005).

$$G = \sqrt{\frac{P}{\mu V}} \tag{1}$$

where μ is the viscosity of the fluid, V the volume of suspension. The power dissipation was obtained from the power number N_p,

$$P = N_p \rho_w n^3 d^5 \tag{2}$$

where ρ_w is the density of the fluid, n represents the stirring frequency in rotations per second and d the diameter of the propeller (Nagata, 1975). The turbulent shear adopted for the study ranged between 5–40 s^{-1} (5.6 s^{-1}, 10 s^{-1}, 16 s^{-1}, 22 s^{-1}, 29 s^{-1}, 40 s^{-1}).

2.1.2. Image capturing system

The flocs formed during the experiments were captured as per the method proposed by Ramalingam and Chandra (2017). The system consists of a DSLR (Digital Single Lens Reflex) camera (Canon 800D), a test section for holding the sample which is placed in a rectangular glass cuvette of 1.5 cm square cross section and 4 cm height, and a LED light of 48 W (Fig. 1) The 18–55 mm normal lens of the camera is converted into a macro-lens with 1 to 4 times magnification using a reverse ring, which disconnects the electronic connection between the lens and the camera, thereby restricting the lens ability to change its aperture. Thus, the aperture, shutter speed and ISO (International Organization for Standardization) has to be set manually and was optimized after a number of trials: Aperture – f/5.0 (f being the focal length), shutter speed – 1/800 & ISO – 3200. An additional light source was required since the macroscopy requires a large amount of illumination, for which a LED light was employed.

2.1.3. Image processing

The captured images were processed using ImageJ software, which is freeware, in order to obtain the floc characteristics. The different stages involved in image processing include: (i) setting scale; (ii) converting image into grey scale; (iii) filtering of image; (iv) thresholding of image; (v) computation of floc characteristics. The process of spatial calibration involves calibrating a single image against known values after which the calibration is applied to un-calibrated image. After calibration, the 24-bit RGB (Red Green Blue) images are compressed into 8-bit grey scale. The grey scale image is further filtered through Fourier transform which involves suppressing or enhancing features in the Fourier domain before carrying out an inverse Fourier transform to obtain a filtered real-space image thereby removing noises and improving the quality of the image. Image thresholding using Otsu's method was employed to reduce the grey-scale image to binary image with the help of an algorithm so that the image get partitioned into foreground and background (Otsu, 1979). Successively, the floc parameters such as area, major axis, minor axis etc. were extracted and the diameter of the floc was obtained, assuming circular cross section (Flory et al., 2004; Mikes et al., 2004; Verney et al., 2009). From the extracted data, the fractal dimension, floc density and floc volume fraction were quantified.

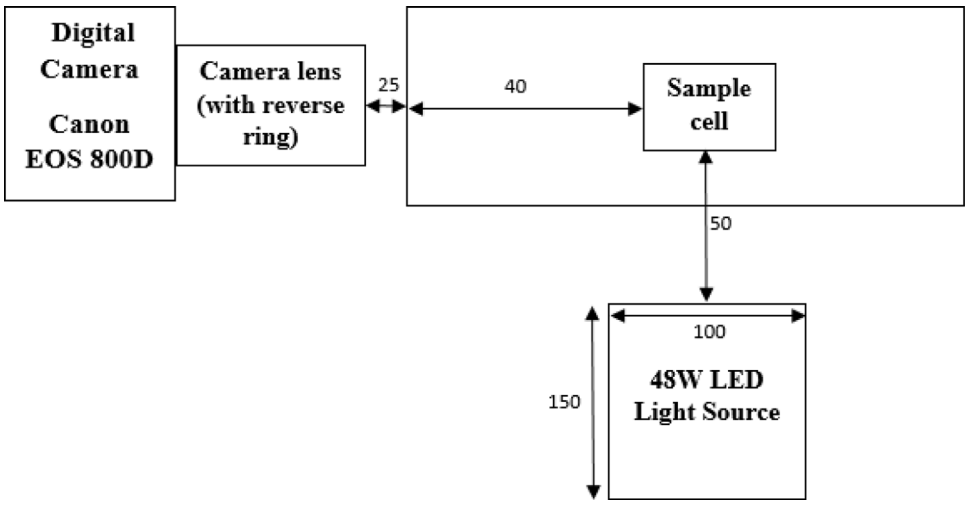

Fig. 1. Image capturing system adopted for the study.

2.2. Experimental protocol

Batch experiments were performed in a 1 L glass beaker in a flocculator using kaolin suspension at a concentration of 1 g/L for all the experimental runs. The particle size distribution of kaolin was analysed using a laser particle size analyser (Analytical) and it was observed that the size varied between 0.1 μm and 4 μm with a d_{50} of 0.6 μm (Fig. 2a). Salinity was varied between 0‰ and 35‰ (0, 5, 10, 15, 20, 25, 30, 35) under varying turbulence shear of 5.6 s^{-1}, 10 s^{-1}, 16 s^{-1}, 22 s^{-1}, 29 s^{-1}, 40 s^{-1} for each salinity. The NaCl of analytical grade was used to vary the salinity values. All experiments were performed for duration of 30 min for ensuring floc formation after which aliquots of 2 mL was pipetted out into a glass cuvette with flat walls for capturing images, as explained earlier. All experiments were repeated in triplicates and the average values were adopted for the analysis of the floc volume fraction (FVF), floc density and breakage coefficient.

Subsequently, experiments were conducted with kaolin suspensions with addition of sand (silica) of analytical grade to examine the influence of non-cohesive sand on the floc break-up. The experiments were conducted at a turbulence of 40 s^{-1} and the flocs formed were characterized. The sand (Akshar Chem Silica Sand – AKSHAR 1124) was added at different proportions ranging between 10% and 50% by weight of kaolin (10%, 20%, 40% and 50%). Fig. 2(b) shows the particle size distribution of silica sand. After 10 min of the addition of sand, aliquots of 2 mL samples were pipetted out into the glass cuvette to analyse the change in the floc characteristics due to the presence of sand. Experiments were repeated in triplicates so as to obtain representative values of floc volume fraction and breakage coefficient for each experimental run.

3. Results and discussion

3.1. Variation of floc sizes with salinity and turbulence

The floc sizes obtained in each set of experiments through routine image capturing and processing methods were used to analyse their dependency on salinity and turbulence. The total count of flocs included in the analysis varied between 20 000 and 35 000. There is a visible variation in the maximum floc size with salinity and turbulence with the maximum size ranging from 766 μm recorded at salinity 10‰ and turbulence shear 10 s^{-1} to 110 μm recorded at salinity 0‰ and turbulence 5.6 s^{-1}. The mean size ranged between 57 μm (at salinity 35‰ and for turbulence 5.6 & 40 s^{-1}) and 79 μm (at salinity 10 ‰ & turbulence 10 s^{-1}). The general trend observed is an increase in the floc size with the initial increase in salinity (from 0‰ to 10‰) and turbulence (5.6 s^{-1} to 10 s^{-1}) and thereafter a gradual reduction in the floc size. The root mean square (RMS) floc size exhibited a variation from 58 μm to 93 μm (Fig. 3(b), whereas the median size have a marginal variation between 52 μm and 63 μm. The highest standard deviation between the floc sizes has been observed for salinity 10‰ for all the turbulence shear.

3.2. Variation of floc density with floc size

The influence of floc size on the density of floc was assessed at a particular turbulence shear of 10 s^{-1}, as this turbulence produced the peak floc size and consists of all ranges of floc size. The density of floc was estimated using the equation proposed by Dyer and Manning (1999) and Mantovanelli and Ridd (2008).

$$\rho_f = \rho_w + (\rho_s - \rho_w)\left(\frac{D_p}{D_f}\right)^{3-n_f} \tag{3}$$

where ρ_w is the density of water, ρ_s the density of particles, D_p the diameter of particle and D_f the equivalent diameter of spherical floc, n_f the fractal dimension, which represent the compactness of floc and corresponds to the slope of log–log variation of area and length of floc.

$$n_f = \frac{\log A}{\log a} \tag{4}$$

where A is the area of the floc and a the major axis of the ellipse containing the floc. Fig. 4 shows the variation of floc density with floc size at various salinity values. It is very well understood that as floc size increases, there is a reduction in the floc density. The floc density ranged between 1.7 g/cc and 1.01 g/cc, the highest being for 4 μm and lowest for 766 μm. The reduction in floc density with floc size is attributed to the formation of more porous structure of floc at higher sizes and this can lead to the easy break-up of floc on the application of turbulence shear. The inverse relationship of floc density with floc size has been proposed by Krone (1963), Winterwerp (1999) and Winterwerp et al. (2006). The influence of salinity on the floc density seem to be very marginal and can be neglected, especially at a salinity >10‰. A marginal increase in floc density has been observed as salinity increased from 0‰ to 10‰. A regression analysis was carried out to establish the relationship between floc size with floc density at a salinity of 10‰, and a power relationship existed

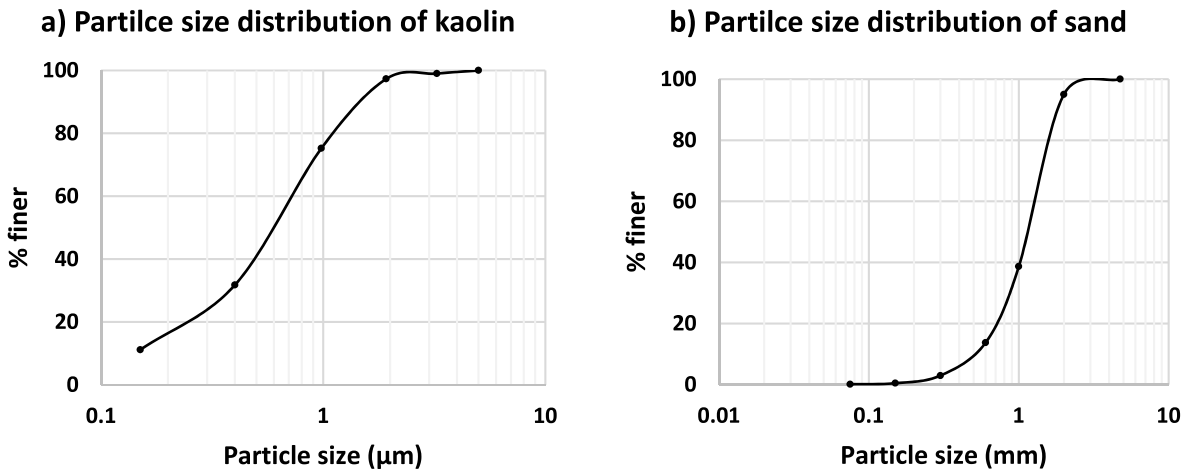

Fig. 2. Particle size distribution of (a) kaolin and (b) sand used for the study.

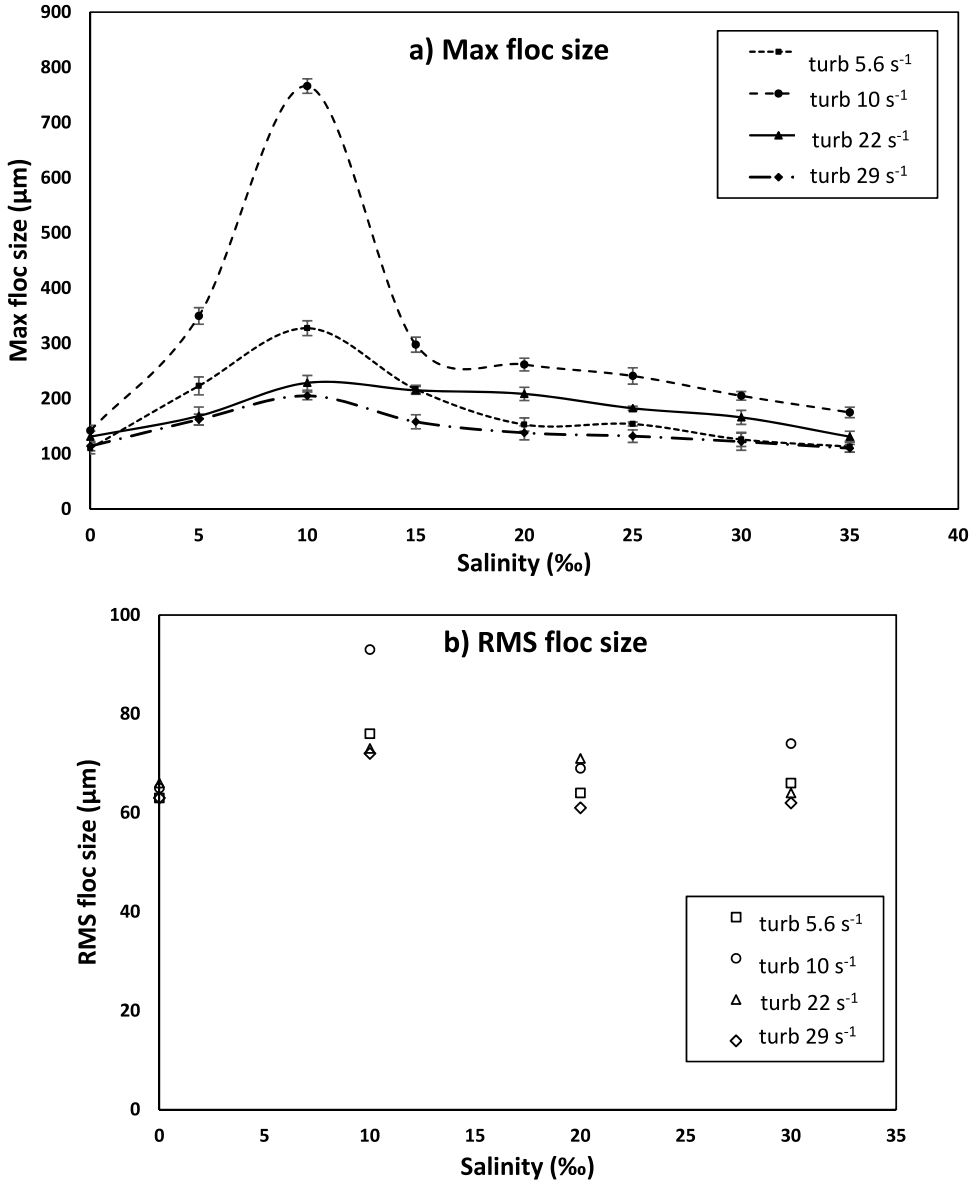

Fig. 3. Variation of (a) Maximum floc size and (b) Root Mean Square (RMS) floc size at various salinity and turbulence shear. *Note: The error bars in Fig. 3(a) represent the standard deviation of the maximum floc size between the triplicate experiments carried out to arrive at the floc size distribution.*

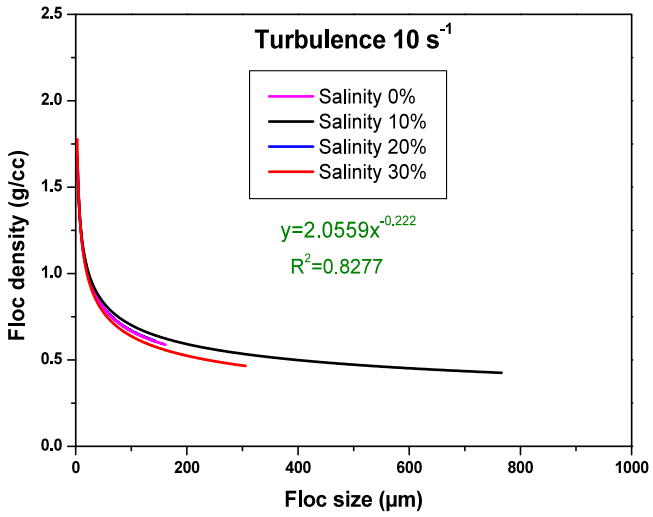

Fig. 4. Variation of floc density with floc size.

for the floc density ρ_f in terms of floc size D_f (as shown in Fig. 4). This relationship finds application while modelling flocculation, where density of floc is an input to the flocculation model. The power relationship between density of floc and floc size takes the form:

$$\rho_f = 2.056{D_f}^{-0.222} \tag{5}$$

3.3. Floc volume fraction of kaolin suspensions

It is highly essential to express the floc population in terms of floc volume fraction rather than representing in terms of floc size and number because it gives a real picture of the volumetric distribution of flocs of different classes. According to the floc size, the flocs are classified into 3 size classes for this study: 0–50 μm, 50–100 μm and >100 μm. The first and second class consists of micro-flocs while the third class forms the macro-floc group. The total volume of flocs in each class divided by the total volume of flocs in all the size classes will give the floc volume fraction of each size class. Fig. 5 shows the floc volume distribution of various size classes at various salinity and turbulence shear. The figure clearly depicts the influence of salinity and turbulence on the floc volume fraction in different size classes. The floc volume fraction exhibited the following variations:

(i) At a salinity of 10‰, the floc volume fraction of size class III (>100 μm) exhibited the highest value for all the turbulence shear; (ii) At higher salinity ranges, the variations of floc volume fraction was marginal for a particular turbulence; (iii) The highest floc volume fraction was obtained for a salinity of 10‰ and a turbulence shear of 10 s^{-1}; (iv) The variations of floc volume fraction for size class II (50–100 μm) was marginal with respect to salinity for a particular turbulence, except for turbulence shear of 10 s^{-1}; (v) the floc volume fraction of size class I (0–50 μm) showed pronounced variations with salinity for all the turbulence shear, wherein micro-floc formation initially decreased and then increased with an increased in salinity. The least population of size class I was recorded at a salinity of 10‰; (vi) As turbulence increased from 5.6 s^{-1} to 10 s^{-1}, floc volume fraction of higher size class (>100 μm) increased, further increase in turbulence resulted in a reduction of floc volume fraction of size class III, while the floc volume fraction of lower class (0–50 μm) reduced initially and further increased with turbulence; (vii) The size class II (50–100 μm) was not much influenced by turbulence, however a marginal decrease in floc volume fraction was evident as the turbulence increased from 5.6 s^{-1} t 10 s^{-1} for the salinity range of 0 ‰– 10‰. From these observations, the following inferences were made:

(1) As the turbulence increase, the macro-floc population initially increases and further decreases; the reason for a decrease being the break-up of macro-flocs into smaller micro-flocs in the size class I (0–50 μm), resulting in an increase in micro-floc population.

(2) The increase in salinity from 0‰ to 10‰ results in an increase in macro-floc population; further increase in the salinity resulted in the flocs to remain as micro-flocs, thus the macro-floc formation is limited by salinity.

3.4. Floc volume fraction of sand-kaolin suspensions

It has been documented that the presence of sand may impart additional shear causing the clay flocs to get fragmented and broken-up (Cuthbertson et al., 2018). In order to quantify the additional shear created by sand, experiments were conducted with sand–clay suspensions at a turbulence of 40 s^{-1} (so as to keep the sand in suspension) and at a salinity of 0‰ and 10‰ (as these salinity ranges play dominant role in floc formation). The floc population initially formed at a turbulence of 40 s^{-1} was obtained and the floc volume fraction after the addition of sand, keeping the turbulence shear constant, was determined. The % changes in the floc volume fraction after the addition of sand at a turbulence of 40 s^{-1} and salinity of 0‰ and 10‰ are represented in Fig. 6. The positive figures show the increase in the floc volume fraction after the addition of sand and vice versa. A pronounced increase in the floc volume fraction of size class I (0–50 μm) and corresponding decrease in the size class III (>100 μm) is observed with an increase in the % sand. This shows that the additional shear created by sand cause the break-up of macro-flocs into micro-flocs. The effect is much prominent at a salinity of 0‰, whereas the flocs formed at salinity 10‰ is comparatively stable and resistant to break-up due to shear imparted by sand. This indicates that the degree of bonding between individual flocs in a macro-floc kernel is much higher at salinity 10‰ than that at salinity 0‰, depicting the role of Van der Waals force of attraction between individual particles at mid-salinity reaches as has been demonstrated by many authors (Van Leussen, 1999; Portela et al., 2013). Thus, the presence of sand in sediment suspension will impart additional shear causing the break-up of macro-flocs.

An analysis of the variation of floc volume fraction of size class III (>100 μm) with turbulence and % sand at salinity 0‰ and 10‰ was attempted (Fig. 7a & b). After the initial build-up of macro-flocs at low turbulence (5.6 s^{-1} to 10 s^{-1}), the floc volume fraction of size class III decreases with further increase in turbulence (Fig. 7a). The relationship for floc volume fraction with turbulence follows a power law relationship for the decreasing limb (Fig. 8). A prominent decrease in the floc volume fraction of size class III was observed with an increase in % sand (Fig. 7b). The floc volume fraction with turbulence for salinity of 0‰ and 10‰ which is obtained through regression analysis as depicted in Fig. 8 is:

$$FVF = 6.66G^{-1.117} \text{ for salinity } 0‰ \tag{6}$$

$$FVF = 27.349G^{-1.39} \text{ for salinity } 10‰ \tag{7}$$

The additional shear created by sand was quantified from the power relationship for the floc volume fraction in terms of turbulence shear (Eqs. (6) and (7)) and is given in Table 1. Here, the floc volume fraction determined experimentally for each % sand was used to derive the equivalent shear caused by sand from the power law relationship (Eqs. (6) and (7)). It was observed that the turbulence shear predicted for salinity 0‰ and 10‰ does not

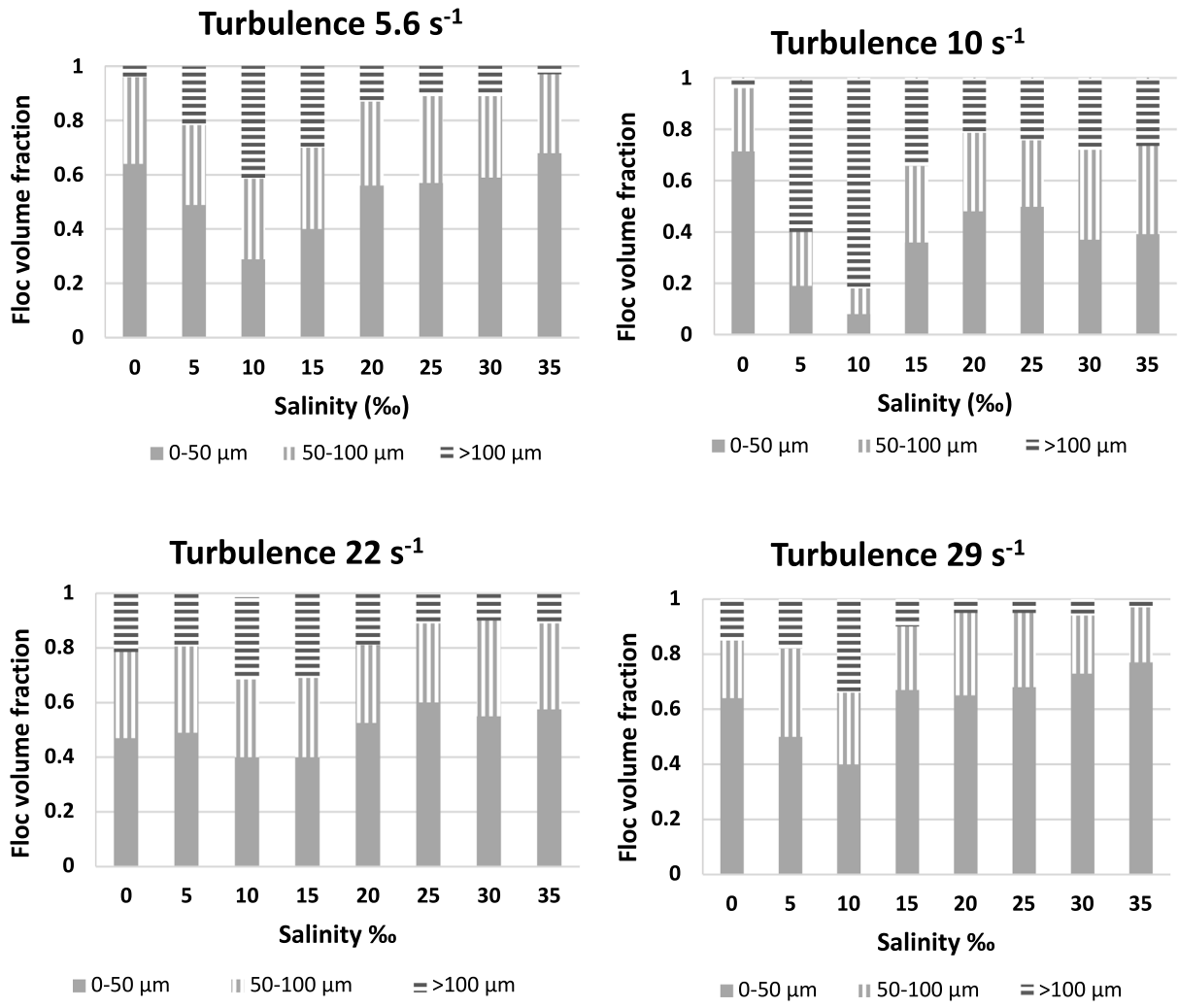

Fig. 5. Floc volume fraction for various size classes at various salinity and turbulence shear.

Table 1
Estimation of turbulence shear caused by sand from the floc volume fraction.

% sand	G (s^{-1})			SD of G
	Salinity 0‰ FVF = $6.66G^{-1.117}$	Salinity 10‰ FVF = $27.349G^{-1.39}$	Average salinity	
10	12	16	14	2.83
20	39	33	36	4.24
40	43	41	42	1.41
50	57	53	55	2.83

vary by more than a standard deviation of 5, thereby implying the reliability of the relationship used for predicting the shear caused due to sand. Thus, the additional shear created by sand varies with % sand as a power law of the form, where S is the % sand in the sediment suspension (Fig. 9).

$$G = 2.69S^{0.78} \tag{8}$$

The variation of floc volume fraction with turbulence shear including that produced by sand is shown in Fig. 10. The influence of salinity on floc volume fraction of size class III is felt only at low turbulence shear, while as the turbulence increases, the effect of salinity becomes weaker. Thus, it is inferred that the influence of salinity on floc formation can be neglected at high turbulence that is high enough to keep the sand in suspension.

3.5. Breakage coefficient

In modelling flocculation of mixed sediments using population balance equation, volume doubling discretization is adopted for the clay fraction (Krishnappan and Marsalek, 2002; Selomulya et al., 2003; Cuthbertson et al., 2018). Accordingly, a floc is assumed to undergo fragmentation resulting in the formation of two equal sized flocs, thereby following binary breakage model, yielding a value of 1/2 for breakage coefficient. Thus, the breakage coefficient, which is the cubic root of ratio of floc volume fraction of a particular size class after breaking to that before breaking, was estimated for flocs of different classes under varying turbulence and % sand. Fig. 11 represents the variation of breakage coefficient with % sand for different size classes, while Fig. 12 that with turbulence (initial part shown in continuous solid line) for size class III (>100 µm). A power law relationship for breakage coefficient Γ in terms of turbulence shear G is proposed:

$$\Gamma = 45.911G^{-1.318} \tag{9}$$

This relationship was used to estimate the breakage coefficient of flocs due to turbulence imparted by sand (Fig. 12). Solid square bullets in the figure represent the predicted breakage coefficient using the power law relationship, while the solid circular bullets show the breakage coefficient determined through experiments. The solid curved line shows the variation of breakage coefficient with applied turbulence shear for average salinity (0‰ and 10‰).

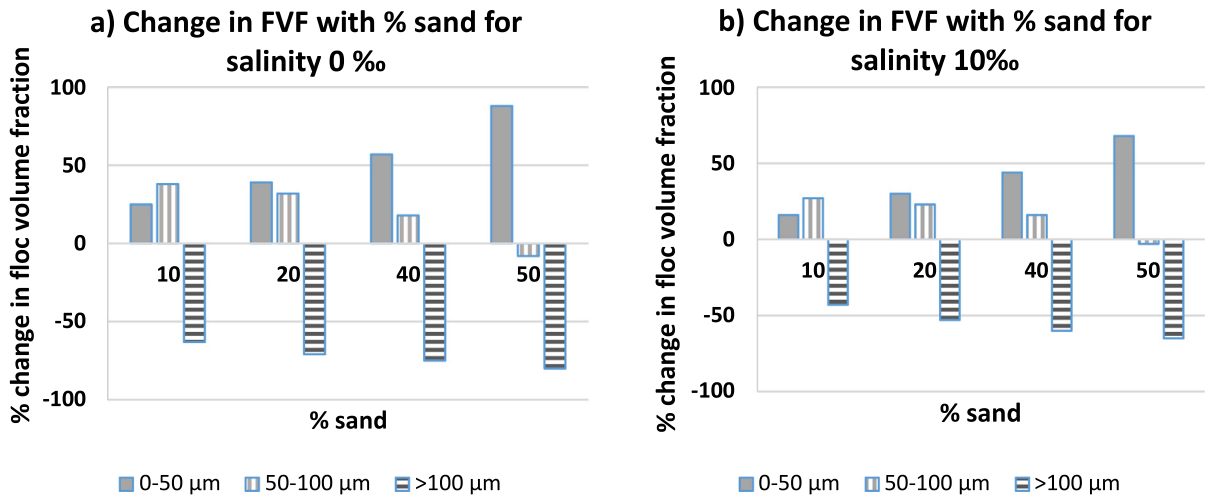

Fig. 6. Change in floc volume fraction with addition of sand for (a) salinity 0‰; (b) salinity 10‰.

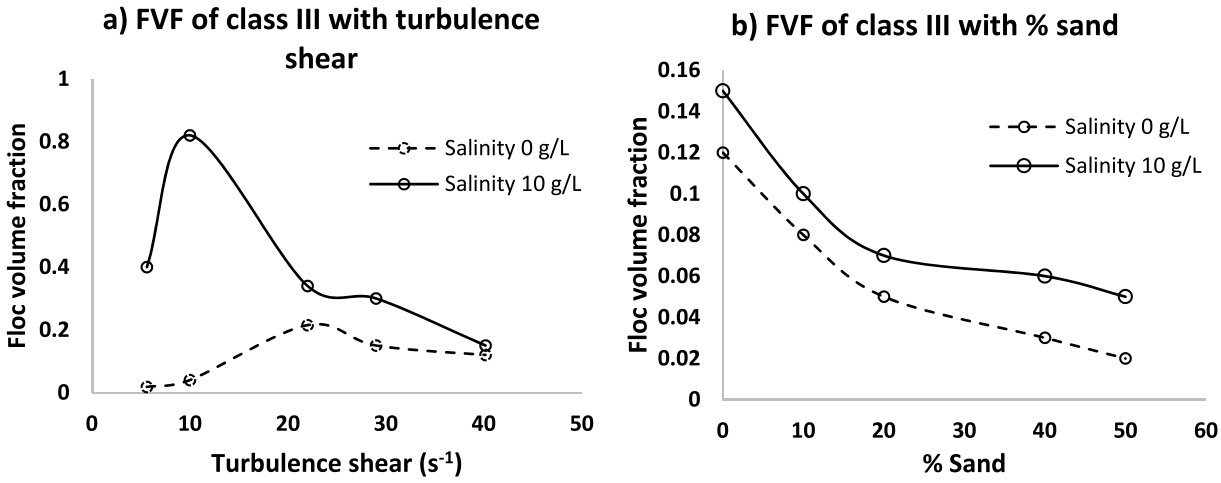

Fig. 7. Variation of floc volume fraction of class III (>100 µm) with (a) turbulence shear; (b) % sand.

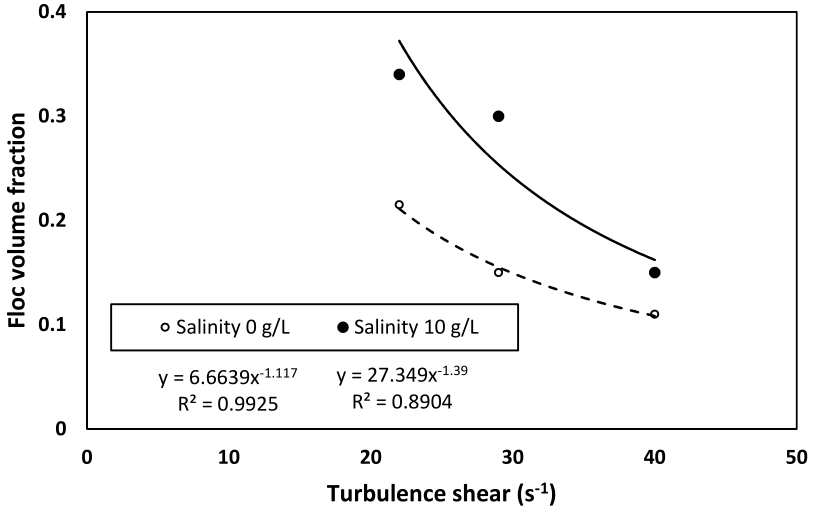

Fig. 8. Decreasing limb of floc volume fraction of class III vs. turbulence curve.

The dotted curved line represents the variation of breakage coefficient of macro-flocs due to turbulence created by sand. It is interesting to note that the dotted curve follows the solid curve, thereby implying that the power law can very well predict the breakage coefficient due to turbulence shear and sand.

A sensitivity analysis was conducted between observed and predicted breakage coefficient of macro-flocs and the results of

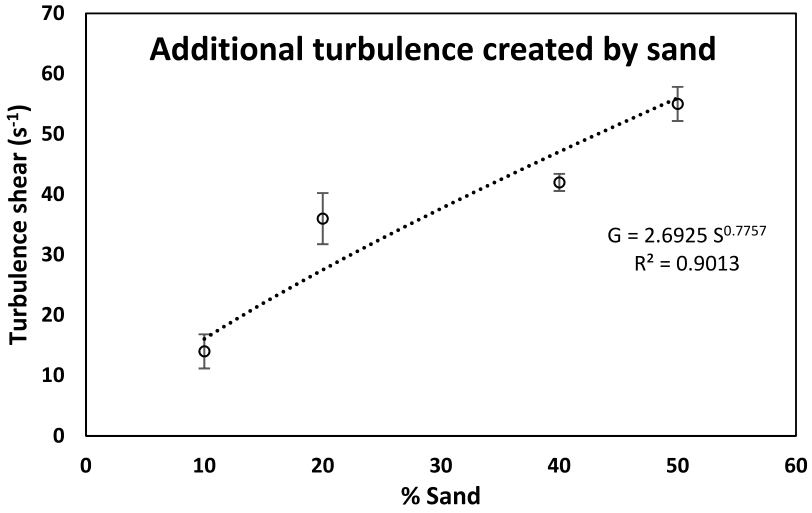

Fig. 9. Turbulence shear created by sand (average of values for salinity 0 and 10‰). *Note: Error bar shows the SD of turbulence shear for salinity 0 and 10‰.*

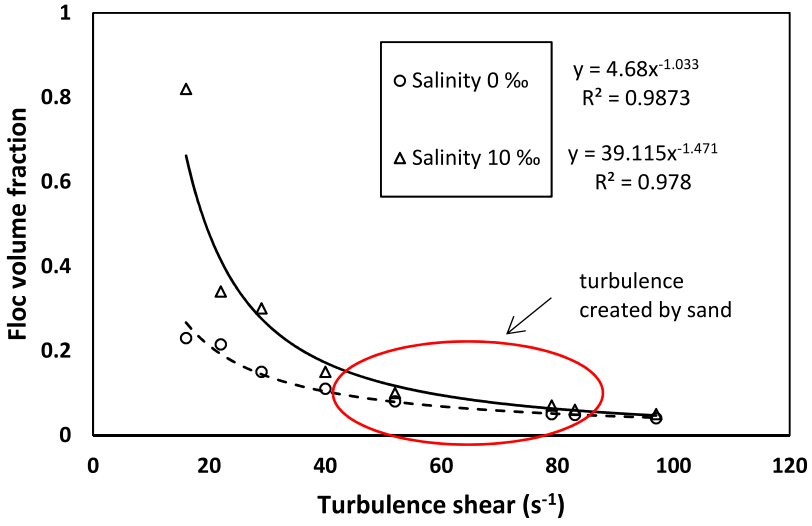

Fig. 10. Variation of floc volume fraction of class III with turbulence (including that caused due to sand) at different salinity; influence of salinity felt only at low turbulence.

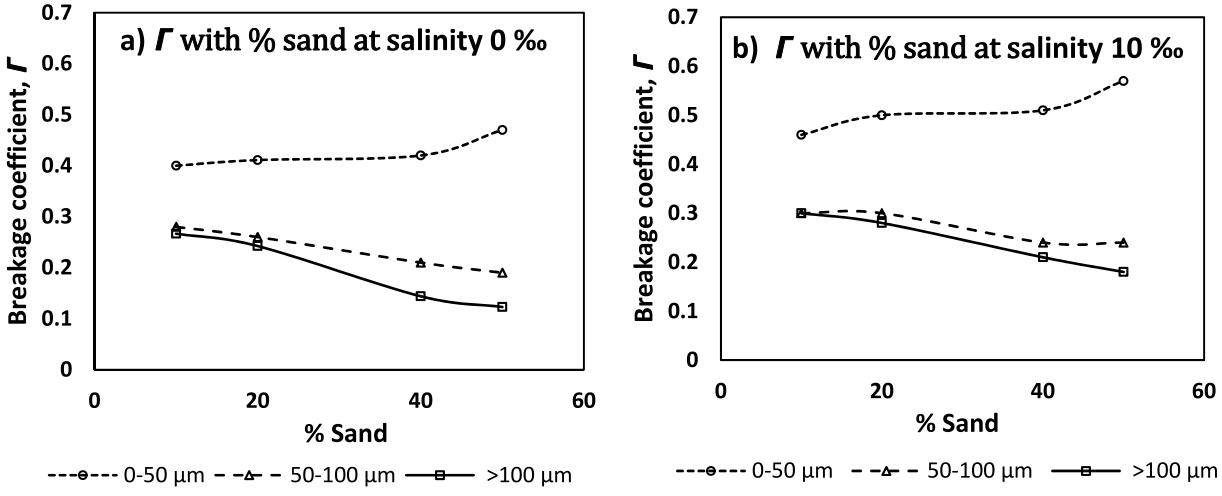

Fig. 11. Breakage coefficient, Γ for flocs of the three size classes for different sand proportion at (a) salinity 0‰ and (b) salinity 10‰.

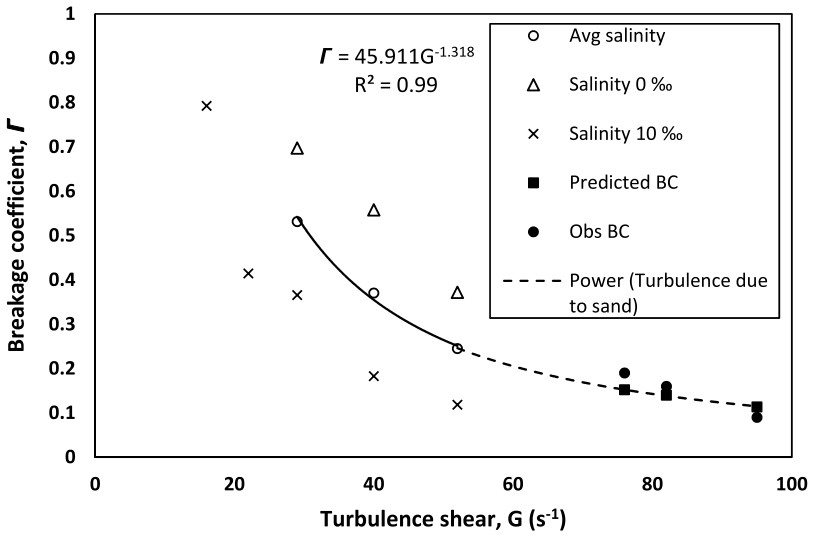

Fig. 12. Breakage coefficient as a function of turbulence (including that created by sand) for size >100 μm. The extended portion of curve shown in dotted line represents the predicted breakage coefficient for flocs >100 μm due to sand induced turbulence.

Table 2
Results of sensitivity analysis.

% sand	G	Breakage coefficient, Γ (predicted)	Breakage coefficient, Γ (observed)	SD	Coefficient of determination (r^2)	Correlation coefficient (r)
20	76	0.152407	0.19	0.03		
40	82	0.14	0.16	0.01	0.9995	0.9997
50	95	0.113574	0.09	0.02		

statistical parameters are presented in Table 2. The power relationship predicted the breakage coefficient of flocs fairly well with a coefficient of determination of 0.99 and a correlation coefficient of 0.99, thereby highlighting the effectiveness of the relationship. Another point that is noteworthy is that the breakage coefficient takes values ranging from 0.8 to 0.1, which indicates that binary breakage model may not be applicable to all ranges of turbulence shear, especially when the sediment consists of cohesionless fraction, wherein the breakage coefficient takes a value less than 0.2. At average turbulence shear conditions, i.e. between 20 and 40 s^{-1}, where most of the estuaries encounter during average tidal conditions, the breakage coefficient approximates to 0.5, during which the binary breakage model finds application. Thus, the study identified that at low turbulence level of <20 s^{-1} and high turbulence level of >40 s^{-1} and in estuaries with mixed sediments, the binary breakage model cannot be applied; the new developed model can very well predict the breakage coefficient. Further, the study highlights that the effect of salinity is negligible at very high turbulence shear conditions and in estuaries having mixed sediment environment. More insight into the settling characteristics are required to further validate the developed relationship for breakage coefficient and is out of scope of the present paper.

4. Conclusions

Microscale investigations were undertaken to investigate the floc characteristics of kaolin suspensions under the influence of salinity, turbulence and non-cohesive sand, which was achieved with the assistance of an image capturing system and image processing, followed by analysis of floc size, fractal dimension, floc density and floc volume fraction in 3 size classes: 0–50 μm, 50–100 μm and >100 μm. The maximum floc size was observed at a salinity of 10‰ and turbulence shear of 10 s^{-1}. The floc density was identified to be a decreasing function of floc size. The floc volume fraction of size class I and III varied with salinity and turbulence, while that of class II was marginal. The floc volume fraction of class III decreases with increase in turbulence shear (above 10 s^{-1}) due to the break-up of macro-flocs, while the floc volume fraction of size class I increases with turbulence. The addition of sand creates additional shear causing the break-up of macro-flocs thereby decreasing the floc volume fraction of size class III with increase in % of sand. The floc volume fraction is a power function of turbulence shear and the power relationship proposed for the floc volume fraction in terms of turbulence, when extended to that due to sand enables the quantification of additional turbulence created by sand. The relationship between the additional turbulence shear and % sand can be applied in estuaries to quantify the turbulence imparted by sand, once the grain size distribution of bed sediments is known, thereby enabling the inclusion of the effect of sand in terms of turbulence while modelling flocculation.

The binary breakage model, which proposes the break-up of a single floc into two equal sized flocs under the influence of turbulence leads to the assumption of breakage coefficient as 1/2. The study suggests that the binary breakage model finds application at intermediate turbulence ranges of 20–40 s^{-1} and cannot be applied in estuaries having bed sediments composed of cohesive and non-cohesive fractions. Thus, the detailed analysis of the breakage coefficient from the experimental results led to the development of a relationship for breakage coefficient in terms of turbulence, which also include the turbulence created by sand. Therefore the developed model can be applied to quantify breakage coefficient under all ranges of turbulence shear encountered in estuaries as well as in estuaries with mixed sediments.

Declaration of competing interest

The authors declare that they have no known competing financial interests or personal relationships that could have appeared to influence the work reported in this paper.

Acknowledgements

The work is funded by TEQIP, Govt of India through Research Seed Money grant. The authors also thank the anonymous reviewers for their constructive comments.

References

Bouyer, D., Escudié, R., Liné, A., 2005. Experimental analysis of hydrodynamics in a jar-test. Process Saf. Environ. Prot. 83 (B1), 22–30.

Burt, T.N., 1986. Estuarine Cohesive Sediment Dynamics: Proceedings of a Workshop on Cohesive Sediment Dynamics with Special Reference to Physical Processes in Estuaries, Tampa, Florida, November 12–14, 1984. In: Lecture Notes on Coastal and Estuarine Studies, vol. 14, Springer, New York, pp. 126–150, chapter Field Settling Velocities of Estuary Muds.

Cuthbertson, A.J.S., Dong, P., Davies, P.A., 2010. Non-equilibrium flocculation characteristics of fine-grained sediments in grid-generated turbulent flow. Coastal Eng. 57 (4), 447–460.

Cuthbertson, A.J.S., Samsami, F., Dong, P., 2018. Model studies for flocculation of sand-clay mixtures. Coast. Eng. 132, 13–32.

Ding, A., Hounslow, M., Biggs, C., 2006. Population balance modelling of activated sludge flocculation: investigating the size dependence of aggregation, breakage and collision efficiency. Chem. Eng. Sci. 61, 63–74.

Dyer, K.R., Manning, A.J., 1999. Observation of the size, settling velocity and effective density of flocs and their fractal dimensions. J. Sea Res. 41, 87–95.

Flory, E.N., Hill, P.S., Milligan, T.G., Grant, J., 2004. The relationship between floc area and backscatter during a spring phytoplankton bloom. Deep Sea Res. I 51, 213–223.

Gratiot, N., Bildstein, A., Anh, T.T., Thoss, H., Denis, H., Michallet, H., Apel, H., 2017. Sediment flocculation in the Mekong river estuary, Vietnam, an important driver of geomorphological changes. C. R. Geosci. 349, 260–268.

Jackson, G., 1995. Comparing observed changes in particle size spectra with those predicted using coagulation theory. Deep-Sea Res. II 42 (1), 159–184.

Krishnappan, B.G., Marsalek, J., 2002. Modelling of flocculation and transport of cohesive sediment from an on-stream stormwater detention pond. Water Res. 36 (15), 3849–3859.

Krone, R.B., 1963. A Study of Rheological Properties of Estuarial Sediments. Report No. 63–68, Hyd. Eng. Lab. and Sanitary Eng. Lab. University of California, Berkeley.

Kusters, K., 1991. The Influence of Turbulence on Aggregation of Small Particles in Agitated Vessels. Eindhoven University of Technology, the Netherlands.

Li, Y., Wolanski, E., Xie, Q., 1993. Coagulation and settling of suspended sediment in the Jiaojiang River estuary, China. J. Coast. Res. 9 (2), 390–402.

Maggi, F., 2005. Flocculation Dynamics of Cohesive Sediment (Ph.D. thesis). University of Technology, Delft.

Manning, A.J., Baugh, J.V., Spearman, J.R., Pidduck, E.L., Whitehouse, R.J.S., 2011. The settling dynamics of flocculating mud-sand mixtures: Part 1—empirical algorithm development. Ocean Dyn. 61 (2–3), 311–350.

Manning, A.J., Baugh, J.V., Spearman, J.R., Whitehouse, R.J.S., 2010. Flocculation settling characteristics of mud: sand mixtures. Ocean Dyn. 60 (2), 237–253.

Mantovanelli, A., Ridd, P.V., 2008. Sedvel: an underwater balance for measuring in situ settling velocities and suspended cohesive sediment concentrations. J. Sea Res. 60, 235–245.

McAnally, W.H., 1999. Aggregation and Deposition of Estuarial Fine Sediment (Ph.D. Thesis). University of Florida, FL.

Mikes, D., Verney, R., Lafite, R., Belorgeym, M., 2004. Controlling factors in estuarine flocculation processes: experimental results with material from the Seine Estuary, Northwestern France. J. Coast. Res. Spec. Issue 41, 82–89.

Nagata, S., 1975. Mixing: Principles and Applications. Halsted Wiley, Chichester.

Otsu, N., 1979. A threshold selection method from gray-level histograms. IEEE Trans. Syst. Man Cybern. 9 (1), 62–66.

Portela, L.I., Ramos, S., Trigo-Teixeira, A., 2013. Effect of salinity on the settling velocity of fine sediments of a harbour basin. In: Conley, D.C., Masselink, G., Russell, P.E., and O'Hare, T.J. (Eds.), Proceedings 12th International Coastal Symposium (Plymouth, England), Journal of Coastal Research, Special Issue No. 65, pp. 1188–1193, ISSN 0749-0208.

Priya, K.L., Jegathambal, P., James, E.J., 2014. Trace metal distribution in a shallow estuary. Toxicol. Environ. Chem. 96 (4), 579–593.

Priya, K.L., Jegathambal, P., James, E.J., 2015. On the factors affecting the settling velocity of fine suspended sediments in a shallow estuary. J. Oceanogr. 71 (2), 163–175.

Priya, K.L., Jegathambal, P., James, E.J., 2016. Salinity and suspended sediment transport in a shallow estuary on the east coast of India. Reg. Stud. Mar. Sci. 7, 88–99.

Ramalingam, S., Chandra, V., 2017. Determination of suspended sediments particle distribution using image capturing method. Mar. Georesour. Geotechnol. 36 (8), 867–874.

Selomulya, C., Bushell, G., Amal, R., White, R.T.D., 2003. Understanding the role of restructuring in flocculation: the application of a population balance model. Chem. Eng. Sci. 58, 327–338.

Spicer, P., Pratsinis, S., 1996. Coagulation-fragmentation: universal steady state particle size distribution. AiChE J. 42, 1612.

Van Leussen, W., 1988. Aggregation of particles, settling velocity of mud flocs: A review. In: Dronkers, J., Van Leussen, W. (Eds.), Physical Processes in Estuaries. Symposium Papers, Sponsored by the Dutch Ministry of Transport and Public Works. Springer-Verlag, Berlin, pp. 427–445.

Van Leussen, W., 1994. Estuarine Macroflocs: Their Role in Fine Grained Sediment Transport. University of Utrecht, Utrecht, p. 488.

Van Leussen, W., 1999. The variability of settling velocities of suspended fine-grained sediment in the Ems estuary. J. Sea Res. 41, 109–118.

Van Leussen, W., Cornelisse, J., 1992. The role of large aggregates in estuarine fine-grained sediment dynamics. In: MEH-TA, A.J. (Ed.), Nearshore and Estuarine Cohesive Sediment Transport. American Geo-physical Union, Washington, DC, pp. 75–91.

Vane, L.M., Zang, G.M., 1997. Effect of aqueous phase properties on clay particle zeta potential and electro-osmotic permeability: Implications for electro-kinetic soil remediation processes. J. Hard Mater. 55, 1–22.

Verney, R., Lafite, R., Brun-Cottan, J.C., 2009. Flocculation potential of estuarine particles: the importance of environmental factors and of the spatial and seasonal variability of suspended particulate matter. Estuar. Coast. 32, 678–693.

Winterwerp, J.C., 1999. On the Dynamics of High-Concentrated Mud Suspension (Ph.D.). University of Technology.

Winterwerp, J.C., 2002. On the flocculation and settling velocity of estuarine mud. Cont. Shelf Res. 22, 1339–1360.

Winterwerp, J.C., Manning, A.J., Martens, C., de Mulder, T., Vanlede, J., 2006. A heuristic formula for turbulence-induced flocculation of cohesive sediment. Estuar. Coast. Shelf Sci. 68, 195–207.

Winterwerp, J.C., Van Kesteren, W.G.M., 2004. Introduction to the physics of cohesive sediment in the marine environment. In: Developments in Sedimentology, Vol. 56. Elsevier, Amsterdam, Netherlands, p. 576.